 CMES, vol.78, no.4, pp.247-275, 2011

A Constitutive Model for Porous Shape Memory Alloys Considering the Effect of Hydrostatic Stress

Bingfei Liu[1], **Guansuo Dui**[1,2] **and Yuping Zhu**[3]

Abstract: A constitutive model considering the effect hydrostatic stresses induced by porosity on the macroscopic behavior of porous Shape Memory Alloys (SMAs) is developed in this paper. First, a unit-cell model is adopted to establish the constitutive relations for the porous SMAs with SMA matrix and the porosity taken to be voids. Dilatational plasticity theory is then generalized for the SMA matrix. Based on an approximation of the velocity field and the upper bound theory, an explicit yield function for the porous SMA is derived from micromechanical considerations. Finally, an example for the uniaxial response under compression of a porous Ni-Ti SMA material under isothermal condition is supplied by using the dense Ni-Ti SMA parameters. Good agreement between the theoretical predictions of the proposed model and published experimental data is observed, and the model can be available to different porosities.

Keywords: Porous shape memory alloys; Yield function; Constitutive model

1 Introduction

Over the last two decades, Shape Memory Alloys (SMAs) have attracted great interests in various fields ranging from aerospace (Jardine et al., 1996; Liang et al., 1996), naval (Garner et al., 2000) and biomedical applications such as surgical instruments (IIyin et al., 1995), medical implants (Martynova et al., 1991) and fixtures (Gyunter et al., 1995) due to their interesting behaviors such as the shape memory effect and superelasticity. Due to this interest, the development of constitutive models for dense SMA have been a topic of many research publications and significant advancements have been reported (Taya et al., 1993; Boyd and Lagoudas, 1994; Lagoudas et al., 1996; Briman, 1997; Pan et al., 2007; Peng et al.,

[1] Institute of Mechanics, Beijing Jiaotong University, Beijing 100044, China
[2] Corresponding author. Tel.: +1-86-1051688437; fax: +1-86-1051682094. E-mail addresses: Gsdui@center.njtu.edu.cn
[3] Institute of Mechanics and Engineering, Jiangsu University, Zhenjiang 100044, China

2008; Wang et al., 2008; Levitas and Ozsoy, 2009; Auricchio et al., 2010; Kim et al., 2010; Arghavani et al., 2011; Phillips et al., 2011;).

Recently, researchers started studying the properties of porous shape memory alloys as they maintain the characteristics of dense SMA such as the shape memory effect, superelasticity, corrosion-resistantance, and biomechanical similarity while also having adjustable mechanical properties, reduced weight and increased biocompatibility due to the addition of porosity (Liu et al., 1997; Otsuka and Ren, 1999; Starosvetsky and Gotman, 2001; Teppei et al., 2005; Greiner et al., 2005). Porous Ni-Ti has been acknowledged as a promising biomaterial for replacing artificial bones or teeth roots as it's mechanical properties can be adjusted to match the tissue it is replacing by adjusting the porosity and associated pore sizes (Lipscomb and Nokes, 1996). Moreover, its porous structure allows body tissues to grow inside and body fluids to be transported through the interconnected pores (Li et al., 2000; Li et al., 2001).

In order to optimally design the microstructure and properties of porous SMAs, it is imperative to develop and implement an accurate model describing its overall properties. Finite element simulations have aided in the understanding of the relationship among pore morphology, overall properties and strain localization (Shen and Brinson, 2007; Panico and Brinson, 2008; Levitas et al., 2009). We want to use micromechanical methods so that many porosities and compositions can be considered without having to make a mesh that is specific to geometry. Micromechanical averaging techniques have been used to investigate the mechanical response of porous SMA (Qidwai et al., 2001; Entchev and Lagoudas, 2002, 2004; Zhao et al., 2005; Nemat-Nasser et al., 2005). Nemat-Nasser et al. (2005) use the parameters with a porosity of 12% to model the superelastic response of the porous Ni-Ti SMA and near to experiments. However, it is hard to reduce to dense case. There is a distinct difference between the predicted results of previous models and the experimental results on the onset of the forward transformation for porous SMAs (Entchev and Lagoudas, 2002, 2004; Zhao et al., 2005). Such discrepancies are due to all these models neglecting the stress concentration due to the pores in the micro-level in determining the onset of transformation. In order to reflect the stress concentration, this work is analyzed by considering the effect of hydrostatic stress. It has been reported by Liu that such stress is important (Liu et al., 2011). It is well known that the phase transformation characteristics of dense SMA are independent of hydrostatic stress, while the macroscopic behavior of porous SMAs are significantly affected by hydrostatic stress (Liu et al., 2011), and the experimental results show that the onset of the phase transformation for porous SMAs occurs earlier than that of dense SMAs (Zhao et al, 2005). Since traditional micromechanical methods (e.g. Mori-Tanaka, dilute, and self-consistent approximations) are based

on the phase average stress, they neglect the effect of stress concentrations caused by the existence of voids. Entchev and Lagoudas, for example, predicted a higher critical stress than experimentally seen (Entchev and Lagoudas, 2002). This is due to they treat the porous SMA as a composite in which the SMA is the matrix and the pores are the inclusions. The effect of hydrostatic stress, however, was not considered. As a result, traditional micromechanical models cannot be used without modification for porous SMAs. Therefore, it is necessary to develop a model accounting for hydrostatic stresses to describe the constitutive relationship of porous SMAs.

Therefore, the objective of this paper is to establish a constitutive model for porous SMAs considering the effect of hydrostatic stress. Similar to Gurson's (1977) approach, we homogenize the microvoids in a SMA matrix to determinine the macroscopic stress in terms of the macroscopic strain-rate and pore volume fraction (PVF). A new yield function is then proposed through both micro and macro scale analysis and the evolution equation for the overall transformation strain is derived using this yield function. The expression for the effective stiffness of the porous SMA material is obtained by considering the SMA as the matrix material and the pores as the inclusions with a stiffness equal to zero. Finally, the uniaxial response predicted by the proposed model is presented and compared with the experimental results of Zhao et al. (2005) showing good agreement.

The remainder of the paper is organized as follows. The constitutive model for dense SMA is briefly reviewed in Section 2. Section 3 then discusses the effect of hydrostatic stress through dilatational plasticity analysis and the yield function for porous SMAs with spherical voids is obtained by upper bound theory. The macroscopic constitutive model for porous SMA is derived in Section 4 based on both the dense SMA model and the pore effect. Section 5 is devoted to simulating the behavior of porous Ni-Ti SMAs and compares the results of the model with available experimental data. Finally, some concluding remarks are given in Section 6.

2 The dense SMA constitutive model

To describe the superelastic behavior of the dense SMA, a constitutive model similar to that developed by Lagoudas et al. (1996) is briefly developed.

Within the framework of small deformations under isothermal conditions, the total strain consists of two parts, an elastic part caused by stress and a transformation strain caused by phase transformation, and is given as,

$$\varepsilon_{ij} = M_{ijkl} : \sigma_{kl} + \varepsilon^t_{ij}, \tag{1}$$

where σ_{kl} and ε_{ij} are the stress and strain tensors, respectively, ε^t_{ij} is the transformation strain tensor, and M_{ijkl} is the compliance tensor defined by the rule of mixtures as

$$M_{ijkl} = M^A_{ijkl} + \xi(M^M_{ijkl} - M^A_{ijkl}) \tag{2}$$

In the above equation, M^A_{ijkl} and M^M_{ijkl} are the compliance tensors of the austenitic and martensitic phases, respectively and ξ is the martensitic volume fraction of dense SMA.

To obtain an evolution equation for ξ, a thermodynamic dissipation potential is utilized. Introducing a dissipation potential $\phi(\sigma'_{ij}, \pi)$, we can get the evolution equation for ξ. The transformation rules and the Kuhn-Tucker optimality conditions (Qidwai and Lagoudas, 2000) are given as follows

$$\dot{\varepsilon}^t_{ij} = \lambda \frac{\partial \phi(\sigma'_{ij}, \pi)}{\partial \sigma'_{ij}} \tag{3}$$

$$\dot{\xi} = \lambda \frac{\partial \phi(\sigma'_{ij}, \pi)}{\partial \pi} \tag{4}$$

$$\begin{aligned} &\dot{\xi} \geq 0, \quad \phi(\sigma'_{ij}, \pi) \leq 0, \quad \dot{\xi}\phi(\sigma'_{ij}, \pi) = 0 \\ &\dot{\xi} \leq 0, \quad \phi(\sigma'_{ij}, \pi) \leq 0, \quad \dot{\xi}\phi(\sigma'_{ij}, \pi) = 0 \end{aligned} \tag{5}$$

where $\sigma'_{ij} = \sigma_{ij} - \sigma_{kk}/3$ is the deviatoric part of the stress σ_{ij}, and π, λ are the generalized thermodynamic force and the Lagrange parameter, respectively. We define the elastic domain as the domain in which no phase transformation occurs. The inequality conditions on $\phi(\sigma'_{ij}, \pi)$ are called the consistency and act as a constraint on the admissibility of the state variables. Conditions expressed by (5) should be satisfied along any loading path. When $\phi(\sigma'_{ij}, \pi) < 0$, (5) enforces the condition $\dot{\xi} = 0$ and the SMA material response is elastic. When $\phi(\sigma'_{ij}, \pi) = 0$ with ξ=0, the SMA material starts phase transformation. The forward phase transformation occurs while $\dot{\xi} > 0$ and reverse transformation occurs while $\dot{\xi} < 0$.

We assume the following function, which is the same to Qidwai and Lagoudas (2000), as the representation of the dissipation potential,.

$$\phi(\sigma'_{ij}, \pi) = [\hat{\phi}(\sigma'_{ij}) + \pi]^2 - Y^2, \tag{6}$$

where Y is the measure of internal dissipation due to microstructural changes resulting from phase transformation and is the critical value necessary for the onset of the phase transformation.

The thermodynamic force conjugate to ξ, π, is given by

$$\pi = \sigma_{ij} : \frac{\partial \hat{\phi}(\sigma'_{ij})}{\partial \sigma'_{ij}} + \frac{1}{2}\sigma_{ij} : (M^M_{ijkl} - M^A_{ijkl}) : \sigma_{kl} + \rho(s^M_0 - s^A_0)T - \frac{\partial f}{\partial \xi} - \rho(u^M_0 - u^A_0) \tag{7}$$

where ρ, s_0 and u_0 are the density, specific entropy and internal energy at the reference state. The superscripts denote the phase they refer to. The function $f(\xi)$ is the hardening function and is given by,

$$f(\xi) = \begin{cases} \frac{1}{2}\rho b^M \xi^2 + (\mu_1 + \mu_2)\xi, & \dot{\xi} > 0 \\ \frac{1}{2}\rho b^A \xi^2 + (\mu_1 - \mu_2)\xi, & \dot{\xi} < 0 \end{cases}, \tag{8}$$

where ρb^M, ρb^A, μ_1, μ_2 are transformation strain hardening constants.
To determine the Lagrange parameter λ, we use the consistency conditions

$$\dot{\phi}(\sigma_{ij},\, \xi) = 0, \quad \frac{\partial \phi}{\partial \sigma_{ij}}\dot{\sigma}_{ij} + \frac{\partial \phi}{\partial \xi}\dot{\xi} = 0. \tag{9}$$

Substituting (4) and (6) into (9), and together with (3), yields the transformation strain evolution equation, which depends on the evolution of the martensitic volume fraction,

$$\dot{\varepsilon}^t_{ij} = \dot{\xi}\frac{\partial \hat{\phi}(\sigma'_{ij})}{\partial \sigma'_{ij}} \tag{10}$$

$$\dot{\xi} = \frac{1}{h}\frac{\partial \hat{\phi}(\sigma'_{ij})}{\partial \sigma'_{ij}}\dot{\sigma}'_{ij}, \tag{11}$$

where,

$$h = \frac{-\partial \pi}{\partial \xi} = \begin{cases} \rho b^M, & when\ \dot{\xi} > 0 \\ \rho b^A, & when\ \dot{\xi} < 0 \end{cases}. \tag{12}$$

The following conditions are obtained for the onset of phase transformation

$$\hat{\varphi}(\sigma'_{ij}) = \begin{cases} Y - \pi, & when\ \dot{\xi} > 0 \\ -Y - \pi, & when\ \dot{\xi} < 0 \end{cases} \tag{13}$$

Let $\hat{\phi}(\sigma'_{ij})$ be defined as (Lagoudas, 1996),

$$\hat{\phi}(\sigma'_{ij}) = H_{\max}\sqrt{3J_2}, \tag{14}$$

where the material parameter $H_{\max}$corresponds to the maximum transformation strain obtained during forward transformation under uniaxial tension and compression and $J_2 = \sigma'_{ij}\sigma'_{ij}/2$ is the second deviatoric stress invariant. The relationship between the transformation strain tensor and the martensitic volume fraction is then given as,

$$\dot{\varepsilon}^t_{ij} = \begin{cases} \dot{\xi}\frac{3H_{\max}\sigma'_{ij}}{2\sqrt{3J_2}} & \text{when } \dot{\xi} > 0 \\ \dot{\xi}\frac{H_{\max}\varepsilon^{t'}_{ij}}{\varepsilon^{t'}_e} & \text{when } \dot{\xi} < 0 \end{cases}, \tag{15}$$

where $\varepsilon^{t'}_{ij}$ is transformation strain at the reversal of the phase transformation and $\varepsilon^{t'}_e = (2\varepsilon^{t'}_{ij}\varepsilon^{t'}_{ij}/3)^{1/2}$.

Using these results, the rate of martensitic volume fraction change can be determined to be,

$$\dot{\xi} = \frac{\dot{\varepsilon}^t_e}{H_{\max}} = \frac{\sqrt{2/3}\sqrt{\dot{\varepsilon}^t_{ij}\dot{\varepsilon}^t_{ij}}}{H_{\max}}. \tag{16}$$

From (1) and (15), we can easily get the relationship between stress and strain for SMAs.

3 The macrostress potential for porous SMA

For porous SMA, the effect of pores must be accounted for. Specifically, the effect of hydrostatic stress will be studied. In order to get the macrostress potential for porous SMA, the following analysis can be used in deriving the yield function for porous SMA, and then the obtained yield function can be used in the constitutive model for porous SMA in next part to respond the macroscopic behavior for porous SMA.

3.1 A unit-cell model for SMA material containing microvoids

A representative volume element of the material under investigation is developed in this part and taken to be a hollow sphere with SMA matrix and the porosity taken to be voids. According to micromechanics (Qu and Cherkaoui, 2006), the porous SMA materials are considered as a composite-sphere model which is subject to a macroscopic stress Σ_{ij} and strain at a rate $\dot{E}_{ij}$. As shown in Fig.1 (a), the composite is assumed to be made of an assembly of composite spheres of various sizes with each composite sphere has a pore of radius a and a SMA shell of thickness$b-a$. The size distribution of the composite spheres must be such that the entire space of the composite is fully occupied by the composite spheres with the presence of

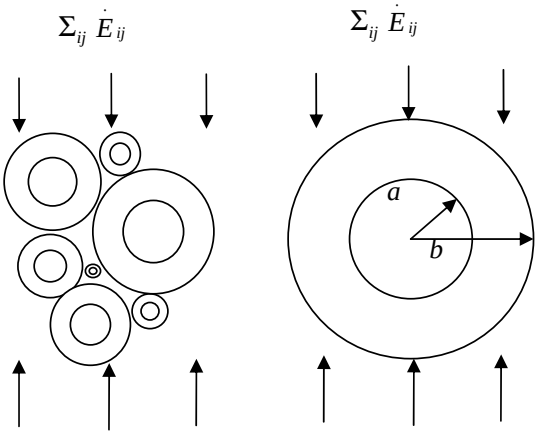

Figure 1: Sketch of the mechanical model

composite spheres of infinitely small sizes. We isolate a typical spherical element of material of radius b which contains a spherical void of radius a as shown in Fig.1 (b) with the same stress and strain in the remote field. The PVF f of the entire composite can be expressed as

$$f = \frac{a^3}{b^3}. \tag{17}$$

Similar to the work of Gurson (1977), the macroscale and microscale are analyzed in this paper. The former refers to the overall cell level on which the microvoids are smeared out in the matrix such that the homogenized material is uniform and compressible, while the latter refers to the level inside the unit-cell where the deformation in the matrix is clearly non-uniform and incompressible. The stress and strain-rate of a RVE are microstress and microstrain-rate fields denoted by σ_{ij} and $\dot{\varepsilon}_{ij}$, respectively. The aim of the present research is to relate the microscopic velocity field to the macroscopic quantities.

The upper bound theorem for finding porous yield criteria has been discussed by Gurson (1977). The desirable velocity field is found by the minimization of the rate of transformation work done.

$$\dot{W} = \frac{1}{V}\int_V \sigma'_{ij}\dot{\varepsilon}^t_{ij}dV \tag{18}$$

where $\dot{\varepsilon}_{ij}^{t}$ is the microscopic transformation strain rate and V is the volume of the unit cell. Define the macroscopic transformation strain rate$\dot{E}_{ij}^{t}$ in terms of the velocity field on the surface of the unit cube. Then the macroscopic stress is related to the microscopic stress and strain rate via

$$\Sigma_{ij} = \frac{\partial \dot{W}}{\partial \dot{E}_{ij}^{t}} = \frac{1}{V}\int_{V} \sigma_{ij}' \frac{\partial \dot{\varepsilon}_{ij}^{t}}{\partial \dot{E}_{ij}^{t}} dV \tag{19}$$

It can be decomposed into the deviatoric part, $\dot{E}_{ij}^{t'}$, and the volumetric part, $\dot{E}_{kk}^{t}\delta_{ij}/3$.

$$\dot{E}_{ij}^{t} = \frac{1}{3}\dot{E}_{kk}^{t}\delta_{ij} + \dot{E}_{ij}^{t'} \tag{20}$$

where δ_{ij} is the Kronecker symbol

$$\delta_{ij} = \begin{cases} 1 & \text{when } i = j \\ 0 & \text{when } i \neq j \end{cases} \tag{21}$$

The microscopic velocity field can be conveniently separated into two parts corresponding to the macroscopic volumetric and deviatoric deformation, respectively.

$$v_i = v_i^s + v_i^v \tag{22}$$

where v_i^s involves shape changes at constant volume and v_i^v involves volume changes at constant shape. By using spherical coordinates and $v_\theta^v = v_\phi^v = 0$, the matrix incompressibility indicates

$$\frac{2v_r^v}{r} + \frac{\partial v_r^v}{\partial r} = a_0 \tag{23}$$

where a_0 represents the volumetric strain rate, the simplest velocity field is assumed $a_0$as constant, when $a_0 = 0$, the above equation reduces to that of Gurson's.

The microscopic velocity field at the surface of the unit cell is connected to the macroscopic transformation strain rate in Cartesian coordinates

$$v_i^s|_s = \dot{E}_{ij}^{t}\, x_j\big|_s, \quad v_i^v|_s = \frac{1}{3}\dot{E}_{kk}^{t}\, x_i|_s \tag{24}$$

The volumetric velocity field becomes

$$v_r^v = \frac{1}{3}\dot{E}_{kk}^{t}\frac{b^3}{r^2}, \quad v_\theta^v = v_\varphi^v = 0 \tag{25}$$

The microscopic transformation strain rate is obtained from the velocity field by

$$\dot{\varepsilon}_{ij}^{t} = \dot{\varepsilon}_{ij}^{tv} + \dot{\varepsilon}_{ij}^{td} \tag{26}$$

where the volumetic strain rate$\dot{\varepsilon}_{ij}^{tv} = (v_{ij}^{v} + v_{ji}^{v})/2$, the deviatoric strain rate$\dot{\varepsilon}_{ij}^{td} = (v_{ij}^{d} + v_{ji}^{d})/2$, and $\dot{\varepsilon}_{kk}^{tv} = \dot{\varepsilon}_{kk}^{td} = 0$.

It is well known that $\dot{\varepsilon}_{ij}^{td}$ does not significantly influence the void growth rate (Huang, 1991). Following Gurson (1977), we approximate the uniform deviatoric strain-rate $\dot{\varepsilon}_{ij}^{td}$ by its macroscopic counterpart

$$\dot{\varepsilon}_{ij}^{td} = \dot{E}_{ij}^{t'} \tag{27}$$

Calculating the $\dot{\varepsilon}_{ij}^{tv}$ in spherical coordinates

$$\begin{aligned}
\dot{\varepsilon}_{rr}^{tv} &= \frac{\partial v_r^v}{\partial r} = \frac{-2}{3}(\frac{b}{r})^3 \dot{E}_{kk}^{t} \\
\dot{\varepsilon}_{\varphi\varphi}^{tv} &= \frac{1}{r}\frac{\partial v_\varphi^v}{\partial \varphi} + \frac{v_r^v}{r} = \frac{1}{3}(\frac{b}{r})^3 \dot{E}_{kk}^{t} \\
\dot{\varepsilon}_{\theta\theta}^{tv} &= \frac{1}{r\sin(\varphi)}\frac{\partial v_\theta^v}{\partial \theta} + \frac{v_r^v}{r} + v_\varphi^v \frac{\cot(\varphi)}{r} = \frac{1}{3}(\frac{b}{r})^3 \dot{E}_{kk}^{t} \\
\dot{\varepsilon}_{r\theta}^{tv} &= \dot{\varepsilon}_{r\varphi}^{tv} = \dot{\varepsilon}_{\varphi\theta}^{tv} = 0
\end{aligned} \tag{28}$$

Then we can write $\dot{\varepsilon}_{ij}^{t}$ in the following form by using a new variable h_{ij}

$$\dot{\varepsilon}_{ij}^{t} = \dot{E}_{ij}^{t'} + \frac{1}{3}\dot{E}_{kk}^{t} h_{ij} \tag{29}$$

In spherical coordinates

$$h_{rr} = -2(b/r)^3 = -2h_{\theta\theta} = -2h_{\phi\phi}, \quad h_{ij}\big|_{i\neq j} = 0 \tag{30}$$

In Cartesian coordinates

$$h_{ij} = (\delta_{ij} - \frac{3x_i x_j}{r^2})(\frac{b}{r})^3 = (\delta_{ij} - 3n_i n_j)(\frac{b}{r})^3 \tag{31}$$

where $r^2 = x_1^2 + x_2^2 + x_3^2$, $n_i = x_i/r$is the Cartesian components to a sphere of radius r.

Combining (19) and (29), and separating into deviatoric and hydrostatic components, we can obtain that the macroscopic stresses under Cartesian coordinates are

related to the microscopic stresses as

$$\begin{aligned}\Sigma'_{ij} &= \frac{1}{V}\int_V \sigma'_{ij}dV \\ \Sigma_{nn} &= \frac{1}{V}\int_V \sigma'_{kl}h_{kl}dV\end{aligned} \tag{32}$$

In spherical coordinates, one can write

$$\Sigma_{nn} = \frac{1}{V}\int_V \frac{3}{2}\sigma'_{rr}h_{rr}dV \tag{33}$$

From (32) and (33), the macroscopic deviatoric stress and the macroscopic hydrostatic stress can be easily calculated from the microscopic quantities in a SMA material containing microvoid. In order to get the macrostress potential for porous SMA, the yield function for porous SMA must be derived base on the microscopic analysis and the model of dense SMA. So the effective stress and the yield function for porous SMA will be discussed in the next part.

3.2 Yield functions

In the Gurson (1977), the matrix material is idealized as rigid-perfectly plastic and the strain hardening constant is not taken into account in. While Tvergaard (1981) have found that the yield function for the voided nonlinear materials does depend on the strain hardening constant. In this work, the SMA matrix will be analyzed by dilatational plasticity theory with a matching strain hardening constant$n$. In simple tension, the effective transformation strain rate and effective stress are related by the power-law formula

$$\frac{\sigma_e}{\sigma_0} = (\frac{\dot{\varepsilon}_e}{\dot{\varepsilon}_0})^n \tag{34}$$

where $\dot{\varepsilon}_0$, σ_0 are the reference strain-rate and stress, respectively and $\dot{\varepsilon}_e = (2\dot{\varepsilon}^t_{ij}\dot{\varepsilon}^t_{ij}/3)^{1/2}$, $\sigma_e = (3\sigma'_{ij}\sigma'_{ij}/2)^{1/2}$ are the equivalent strain rate and the equivalent stress. One matching strain hardening constant$n$among 0 and 1 is for the SMA matrix.

For multiaxial state of stress, we define a potential of the stress as follows

$$\dot{w}(\dot{\varepsilon}^t_{ij}) = \frac{\dot{\varepsilon}_0\sigma_0}{n+1}(\frac{\dot{\varepsilon}_e}{\dot{\varepsilon}_0})^{n+1} \tag{35}$$

The stress is $\sigma_{ij} = \partial \dot{w}(\dot{\varepsilon}^t_{ij})/\partial \dot{\varepsilon}^t_{ij}$. Then we can easily find the relationship between transformation strain-rate and the deviatoric stress, that is

$$\sigma'_{ij} = \frac{2\sigma_0}{3}(\frac{\dot{\varepsilon}_e}{\dot{\varepsilon}_0})^{n-1}\frac{\dot{\varepsilon}^t_{ij}}{\dot{\varepsilon}_0} \tag{36}$$

Substituting (36) into (32), (33) and (18), we express the macroscopic stresses and the macroscopic dissipation for porous SMA as

$$\Sigma'_{ij} = \frac{1}{V}\int_V \frac{2}{3}(\frac{\sqrt{2\dot{\varepsilon}^t_{ij}\dot{\varepsilon}^t_{ij}/3}}{\dot{\varepsilon}_0})^{n-1}\frac{\sigma_0\dot{\varepsilon}^t_{ij}}{\dot{\varepsilon}_0}dV \tag{37}$$

$$\Sigma_{nn} = \frac{1}{V}\int_V (\frac{\sqrt{2\dot{\varepsilon}^t_{ij}\dot{\varepsilon}^t_{ij}/3}}{\dot{\varepsilon}_0})^{n-1}\frac{\sigma_0\dot{\varepsilon}^t_{rr}h_{rr}}{\dot{\varepsilon}_0}dV \tag{38}$$

$$\dot{W} = \frac{1}{V}\int_V \frac{2}{3}\sigma_0(\frac{\sqrt{2\dot{\varepsilon}^t_{ij}\dot{\varepsilon}^t_{ij}/3}}{\dot{\varepsilon}_0})^{n-1}\frac{\dot{\varepsilon}^t_{kl}\dot{\varepsilon}^t_{kl}}{\dot{\varepsilon}_0}dV \tag{39}$$

Introduce the average effective stress in the matrix material by

$$\bar{\sigma}_e = \frac{1}{V_m}\int_{V_m}\sigma_e dV_m = \frac{1}{V_m}\int_{V_m}\sigma_0(\frac{\dot{\varepsilon}_e}{\dot{\varepsilon}_0})^n dV_m \tag{40}$$

According to (30), we use the coordinate transformation $\dot{E}^{t'}_{ij}n_i n_j\Big|_{cartesian} = \dot{E}^{t'}_{rr}\Big|_{spherical}$ to give

$$\dot{\varepsilon}^t_{ij}\dot{\varepsilon}^t_{ij} = \dot{E}^{t'}_{ij}\dot{E}^{t'}_{ij} - 2\dot{E}^t_{mm}\dot{E}^{t'}_{rr}(\frac{b}{r})^3 + \frac{2}{3}\dot{E}^{t2}_{mm}(\frac{b}{r})^6 \tag{41}$$

The next step is to find the approximate analytic solutions to (37), (38), (39) and (40), because they can be combined to give an approximate yield function for porous SMA. The functions F, G, H, I, J, and K are defined in Appendix A to simplify the equations. The method used for solving the present issue is to expand the functions in $\mu = \dot{E}^{t'}_{rr}/\sqrt{2\dot{E}^{t'}_{kl}\dot{E}^{t'}_{kl}/3}$ around $\mu = 0$, then integrate over Ω. The expansions are used because they are too complicated for exact integration and there is a good accuracy result from truncating the expansions after the second order term in μ. The detailed derivation is given in Appendix A.

$$\dot{W} = \frac{\sigma_0(\dot{E}^{t'}_{mn}\dot{E}^{t'}_{mn})^{(n+1)/2}}{\dot{\varepsilon}^n_0}(\frac{2}{3})^{(n+1)/2}(\bar{I}^{(0)} + \frac{1}{10}\bar{I}^{(2)} - \frac{1}{20D}\bar{J}^{(1)} + \frac{2}{5}\bar{H}^{(0)} + \frac{1}{20}\bar{H}^{(2)})$$

(42)

$$\frac{\Sigma'_{ij}}{\sigma_0} = \frac{(\dot{E}^{t'}_{mn}\dot{E}^{t'}_{mn})^{n/2}}{\dot{\varepsilon}_0^n}(\frac{2}{3})^{n/2}t_{ij}(\frac{2}{3}\bar{F}^{(0)} + \frac{1}{15}\bar{F}^{(2)}) \tag{43}$$

$$\frac{\Sigma_{kk}}{\sigma_0} = \frac{(\dot{E}^{t'}_{mn}\dot{E}^{t'}_{mn})^{n/2}}{\dot{\varepsilon}_0^n}(\frac{2}{3})^{n/2}(4D\bar{H}^{(0)} + \frac{2D}{5}\bar{H}^{(2)} - \frac{2}{5}\bar{G}^{(1)}) \tag{44}$$

$$\bar{\sigma}_e = \sigma_0\frac{(\dot{E}^{t'}_{mn}\dot{E}^{t'}_{mn})^{n/2}}{\dot{\varepsilon}_0^n}(\bar{K}^{(0)} + \frac{2}{5}\bar{K}^{(2)}) \tag{45}$$

where $\Sigma_{eq} = (3\Sigma'_{ij}\Sigma'_{ij}/2)^{1/2}$, $\Sigma'_{ij} = \Sigma_{ij} - \Sigma_{kk}/3$, $\Sigma_m = \Sigma_{kk}/3$ are the effective stress, the deviatoric part of the macroscopic Cauchy stress tensor Σ_{ij} and the hydrostatic pressure. Afterwards, again neglecting higher terms, we can calculate the macroscopic stresses and the macroscopic dissipation to

$$\dot{W} = \frac{\sigma_0(\dot{E}^{t'}_{mn}\dot{E}^{t'}_{mn})^{(n+1)/2}}{\dot{\varepsilon}_0^n}(\frac{2}{3})^{(n+1)/2}(\bar{I}^{(0)} + \frac{2}{5}\bar{H}^{(0)}) \tag{46}$$

$$\frac{\Sigma_{eq}}{\sigma_0} = \frac{(\dot{E}^{t'}_{mn}\dot{E}^{t'}_{mn})^{n/2}}{\dot{\varepsilon}_0^n}(\frac{2}{3})^{n/2}\left|\bar{F}^{(0)}\right| \tag{47}$$

$$\frac{3\Sigma_m}{2\sigma_0} = \frac{(\dot{E}^{t'}_{mn}\dot{E}^{t'}_{mn})^{n/2}}{\dot{\varepsilon}_0^n}(\frac{2}{3})^{n/2}2D\bar{H}^{(0)} \tag{48}$$

$$\bar{\sigma}_e = \sigma_0\frac{(\dot{E}^{t'}_{mn}\dot{E}^{t'}_{mn})^{n/2}}{\dot{\varepsilon}_0^n}\bar{K}^{(0)} \tag{49}$$

Compression of the approximate solution (47), (48) to (43), (44) at $f = 0.05$, $n = 0$ is displayed in Fig.2. Dot curve represents the approximate result and solid curve corresponds to (43), (44). As seen in Fig.2, it is observed that the approximate solution agrees very well with the model considering the second term. So the expansion is reasonable in the present model.

The analytical solution of the yield function Φ_n should derived by (47) and (48) with the strain hardening constant n. Using above, we can discuss several limits of the yield functions. These limits play an important role in constituting the approximate analytical solution and analyzing constitutive relations for porous shape memory alloys.

In the limits as$n = 0$, the model can be degenerated to Gurson's model, and (A7), (A8) in Appendix A become

$$\int_1^{1/f}\frac{Q^{-1/2}}{x^2}dx = \frac{-Q}{x} + 2D\mu G(x,\mu) = F(x,\mu) \tag{50}$$

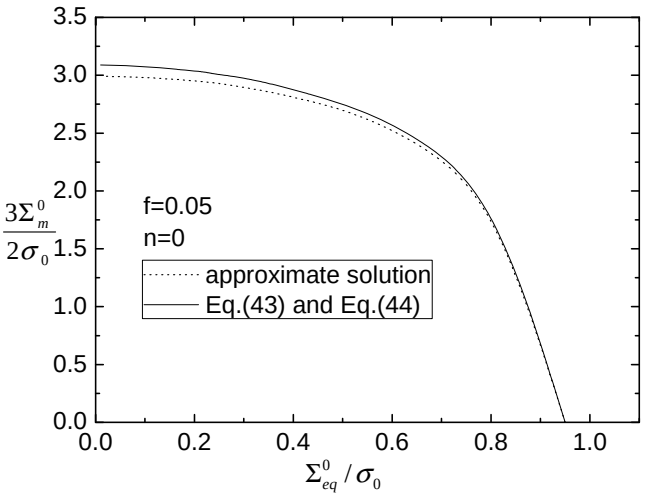

Figure 2: Comparison of model approximate solution and the result of (43) and (44) for strain hardening constant of 0 for a PVF of 0.05.

$$\int_1^{1/f} \frac{Q^{-1/2}}{x} dx = -\ln[\frac{Q^{1/2}+1}{x} - 2D\mu] = G(x,\mu) \tag{51}$$

$$\int_1^{1/f} Q^{-1/2} dx = \frac{1}{2|D|} \ln[Q^{1/2} - 2D\mu] = H(x,\mu) \tag{52}$$

$$\frac{x}{2} Q^{1/2} \,|_1^{1/f} = I(x,\mu), \quad Q^{1/2} \,|_1^{1/f} = J(x,\mu), \quad 1 = K(x,\mu) \tag{53}$$

Then, the approximate stress integrals (46), (47), (48) and (49) become to

$$\dot{W}_0 = \frac{\sigma_0 (\dot{E}^{t'}_{mn} \dot{E}^{t'}_{mn})^{1/2}}{\sqrt{3/2}} \{ \frac{1}{2f} \sqrt{1 + \frac{4D^2}{f}} - \frac{1}{2} \sqrt{1^2 + 4D^2} + \frac{1}{5|D|} \ln[\frac{(f^2+4D^2)^{1/2} + 2|D|}{f[(1+4D^2)^{1/2} + 2|D|]}] \} \tag{54}$$

$$\frac{3\Sigma_m}{2\sigma_0} = \ln\{ \frac{(f^2+4D^2)^{1/2} + 2|D|}{f[(1+4D^2)^{1/2} + 2|D|]} \} \tag{55}$$

$$\frac{\Sigma_{eq}}{\sigma_0} = \sqrt{1+4D^2} - \sqrt{f^2+4D^2} \tag{56}$$

$$\bar{\sigma}_e = \sigma_0 \tag{57}$$

Thus the yield function for the spherical geometry is

$$\Phi_0 = (\frac{\Sigma_{eq}}{\sigma_0})^2 + 2f\cosh(\frac{3}{2}\frac{\Sigma_m}{\sigma_0}) - 1 - f^2 = 0 \tag{58}$$

This function shows that the result is the same as Gurson's model. In this case, the SMA matrix is treated as a rigid-perfectly plastic material with the strain hardening constant $n = 0$, andσ_0 is taken as the yield stress of the SMA matrix material.

In the limits as$n$ = 1, (A7) and (A8) in Appendix A become

$$\int_1^{1/f} \frac{1}{x^2}dx = F(x,\mu), \quad \int_1^{1/f} \frac{1}{x}dx = G(x,\mu), \quad \int_1^{1/f} 1dx = H(x,\mu) \tag{59}$$

$$\frac{x}{2}Q\,|_1^{1/f} = I(x,\mu), \quad Q\,|_1^{1/f} = J(x,\mu), \quad \int_{1-f}^{(1-f)/f} \frac{Q^{1/2}}{x^2}dx = K(x,\mu) \tag{60}$$

In the same way, the yield function for the spherical geometry is describe as

$$\Phi_1 = (\frac{\Sigma_{eq}}{\bar{\sigma}_e})^2 + f(\frac{3}{2}\frac{\Sigma_m}{\bar{\sigma}_e})^2 - (1-f)^2 = 0 \tag{61}$$

In this case, the SMA matrix is treated as a linear viscous material with the strain hardening constant $n = 1$, and $\bar{\sigma}_e$ is taken as the average effective stress of the SMA matrix material.

4 Constitutive model for porous SMA

To describe the mechanical behavior of porous SMA, we now generalize constitutive equations to include elasticity and phase transformation strain hardening. Based on the analysis of micromechanics, the development of the constitutive model is analyzed by considering the porous SMA as a two-phase composite material with SMA as the matrix and pores as the inclusion. Under condition of isothermal, the effective mechanical response is the same as that for the dense SMA in (1). Subsequently, the macroscopic strain rate can be decomposed as the sum of elastic and phase transformation part.

$$\dot{E}_{ij} = M_{ijkl} : \dot{\Sigma}_{kl} + \dot{E}^t_{ij} \tag{62}$$

where $M_{ijkl} = M^I_P$ is the compliance tensor for porous SMA, and the superscripts $I = A$, M, m stand for austenite, martensite and the mixed phase, respectively. By

considering the existence of the spherical pores and using Mori-Tanaka mean-field theory (Tanaka, 1986), the Young's modulus of a porous Ni-Ti SMA can be fully represented by (Mochida et al., 1991).

$$L_P^I = \frac{7-7f}{7+8f}(L_D^A + \zeta(L_D^M - L_D^A)) \tag{63}$$

where L_D^A, L_D^M are the Young's moduli of austenite and martensite phase for dense SMA, respectively. ζ is the martensite volume fraction of porous SMA.

The rate of the martensitic volume fraction for the dense SMA is given by (16). As for porous SMA, combining (16) and (41), we deduce the rate of the martensitic volume fraction immediately as follows

$$\dot{\zeta} = \frac{1}{V_m}\int_{V_m} \dot{\xi} dV_m = \frac{1-f}{H_{\max}}\frac{\dot{W}_0}{\sigma_0} \tag{64}$$

where $\dot{W}_0$ is evaluated by (54). Thus the variation of martensitic volume fraction is proportional to the macroscopic dissipation at $n = 0$ in accordance with (63). From (16) and (63), we can approximate get the maximum transformation strain for porous SMA is

$$H_{\max}^P = \frac{H_{\max}}{1-f} \tag{65}$$

Since it is hard to find the analytic solution for $0 < n < 1$ on (47) and (48), an approximate one for the yield function is needed. It must be associated with the PVF f and the strain hardening constant n. Similar to Wang et al. (1995), in order to get the good agreement between the approximate yield function and analytical expression of the yield function (47), (48), we induce an adjusted coefficient$q$, and the approximate yield function can be expressed numerically by

$$\Phi_n = (\frac{\Sigma_{eq}}{\bar{\sigma}})^2 + 2f\cosh(\frac{3}{2}(\frac{\Sigma_m}{\bar{\sigma}})^{\frac{1}{qn+1}}) - 1 - f^2 = 0 \tag{66}$$

Comparisons between the analytical expression of the yield function (47), (48) and the approximate equation (65) are carried out with different values of the strain hardening constant$n$ and the PVFf. Numerical results show that for $n > 0.5$ taking $q = 0.73$gives a very good agreement between (47) and (65). For$n \leq 0.5$, it is numerically suggested that $q = 0.8$ is a reasonably good approximate of the analytical expression. $\bar{\sigma}$ is the average effective stress value in the SMA matrix. For the hardening response of porous SMA we will use the simple form by

$$\bar{\sigma} = \begin{cases} \sigma_s^M + h\varsigma, & when\ \ \dot{\varsigma} > 0 \\ \sigma_s^A - h\varsigma, & when\ \ \dot{\varsigma} < 0 \end{cases}, \quad \sigma_0 = \bar{\sigma}|_{\varsigma=0} \tag{67}$$

here h is defined same as that in the dense SMA by (12), σ_s^M and σ_s^A stand for the critical stresses necessary to start transformation for martensite and austenite state, respectively.

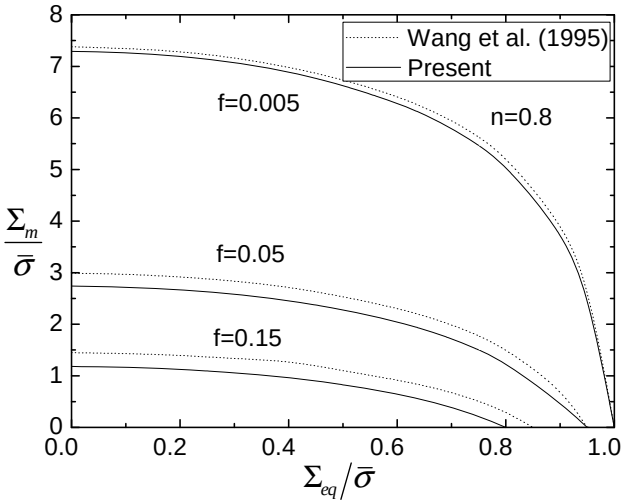

Figure 3: Comparison of model and Wang's approximate yield function for strain hardening constant of 0.8 for PVFs of 0.005, 0.05 and 0.15.

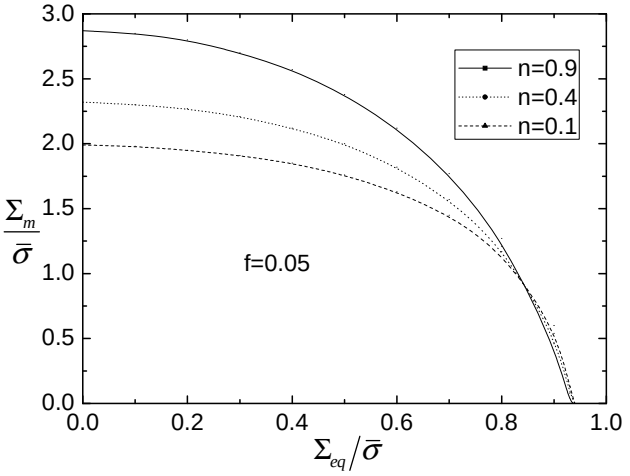

Figure 4: Comparison of model yield surfaces for strain hardening constants of 0.1, 0.4 and 0.9 for a PVF of 0.05.

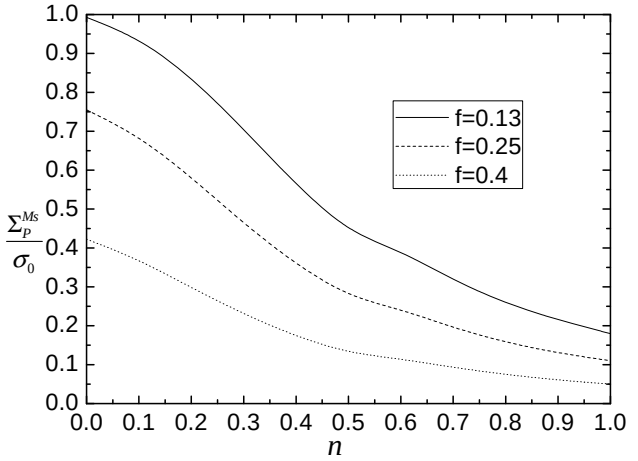

Figure 5: Comparison of model critical phase transformation stresses for versus strain hardening constants for PVFs of 0.13, 0.25 and 0.4.

Fig.3 gives a comparison between the approximate yield function (65) and Wang et al. (1995) with the strain-hardening exponent $n = 0.8$ for$f = 0.005$ $f = 0.05$ and $f = 0.15$, respectively. It is shown that the shapes of the curve modeled by (65) and Wang's are similar to each other, especially for small values of f. The dependence of the yield surface (65) on the strain hardening exponent at $f = 0.05$ is displayed in Fig.4. It indicates that the yield function has a strong n-dependence. What's more, the yield surface is expanding with the increasing of the value n.

The critical phase transformation stress of the start martensitic transformation for porous SMA can be calculated by the yield condition (65). If $\Phi_n = 0$, the phase transformation occurs. At this time, the applied stress is just equal to the start martensitic transformation stress. According to the above analysis, we can easily evaluate the critical phase transformation stress Σ_P^{Ms} for the porous SMA by (65) at the case of $\bar{\sigma} = \sigma_0$. The critical phase transformation stresses for porous SMA with different porosities are shown in Fig.5. As seen in Fig.5, the values of critical phase transformation stresses under different porosities reflect the fact that raising the porosity decreases the start value of martensite transformation.

In generalizing the case to include elastic part and transformation strain-hardening, one has the flexibility in choosing suitable transformation rules for SMA matrix different from the associated one. The increment of overall phase transformation strain during the forward or reverse phase transformation can be expressed as

$$\dot{E}_{ij}^t = \Lambda \frac{\partial \Phi_n}{\partial \Sigma_{ij}} \tag{68}$$

where Λ is a macroscopic scalar, determined by the consistency conditions

$$\dot{\Phi}_n(\Sigma_{ij},\ \varsigma,\ f)=0,\quad \frac{\partial\Phi_n}{\partial\Sigma_{ij}}\dot{\Sigma}_{ij}+\frac{\partial\Phi_n}{\partial\varsigma}\dot{\varsigma}+\frac{\partial\Phi_n}{\partial f}\dot{f}=0 \tag{69}$$

where

$$\frac{\partial\Phi_n}{\partial\Sigma_{ij}}=\frac{3\Sigma'_{ij}}{\bar{\sigma}^2}+f\frac{1}{\bar{\sigma}}\frac{1}{qn+1}\sinh[\frac{3}{2}(\frac{\Sigma_m}{\bar{\sigma}})^{\frac{1}{qn+1}}](\frac{\Sigma_m}{\bar{\sigma}})^{\frac{-nq}{qn+1}}\delta_{ij} \tag{70}$$

$$\frac{\partial\Phi_n}{\partial f}=2\cosh[\frac{3}{2}(\frac{\Sigma_m}{\bar{\sigma}})^{\frac{1}{qn+1}}]-2f \tag{71}$$

$$\frac{\partial\Phi_n}{\partial\varsigma}=\begin{cases}\frac{\partial\Phi_n}{\partial\bar{\sigma}}\rho b^M & when\ \ \dot{\xi}>0\\ -\frac{\partial\Phi_n}{\partial\bar{\sigma}}\rho b^A & when\ \ \dot{\xi}<0\end{cases} \tag{72}$$

Subsequently, the macroscopic dissipation can also be expressed by

$$\dot{W}=\Sigma_{eq}\dot{E}^t_{eq}+\Sigma_m\dot{E}^t_{kk} \tag{73}$$

where the normal transformation rule is

$$\dot{E}^t_{eq}=\Lambda\frac{\partial\Phi_n}{\partial\Sigma_{eq}},\quad \dot{E}^t_{kk}=\Lambda\frac{\partial\Phi_n}{\partial\Sigma_m} \tag{74}$$

Substituting (72) and (73) into (63), together with (46) and (54), we can find the expression of the approximate evolution equation for the martensitic volume fraction ς.

$$\dot{\varsigma}=\frac{\Lambda(1-f)}{H_{\max}\bar{\sigma}}(\Sigma_{eq}\frac{\partial\Phi_n}{\partial\Sigma_{eq}}+\Sigma_m\frac{\partial\Phi_n}{\partial\Sigma_m}) \tag{75}$$

The evolution equations for f is taken as that by Gurson (1977)

$$\dot{f}=(1-f)\dot{E}^t_{kk}=(1-f)\Lambda\frac{\partial\Phi_n}{\partial\Sigma_m} \tag{76}$$

Substitution of (74) and (75) back into (68) leads to

$$\Lambda=\frac{\frac{\partial\Phi_n}{\partial\Sigma_{ij}}\dot{\Sigma}_{ij}}{-\frac{\partial\Phi_n}{\partial\varsigma}\frac{1-f}{H_{\max}\bar{\sigma}}(\Sigma_{eq}\frac{\partial\Phi_n}{\partial\Sigma_{eq}}+\Sigma_m\frac{\partial\Phi_n}{\partial\Sigma_m})-(1-f)\frac{\partial\Phi_n}{\partial f}\frac{\partial\Phi_n}{\partial\Sigma_m}} \tag{77}$$

Let H be

$$H=-\frac{\partial\Phi_n}{\partial\varsigma}\frac{1-f}{H_{\max}\bar{\sigma}}(\Sigma_{eq}\frac{\partial\Phi_n}{\partial\Sigma_{eq}}+\Sigma_m\frac{\partial\Phi_n}{\partial\Sigma_m})-(1-f)\frac{\partial\Phi_n}{\partial f}\frac{\partial\Phi_n}{\partial\Sigma_m} \tag{78}$$

In conjunction with the elastic strain-rate, the constitutive equation (61) can be inverted to give

$$\dot{E}_{ij} = [\frac{1+\upsilon}{2L_P^I}(\delta_{ik}\delta_{jl}+\delta_{il}\delta_{jk}) - \frac{\upsilon}{L_P^I}\delta_{ij}\delta_{kl} + \frac{1}{H}\frac{\partial\Phi_n}{\partial\Sigma_{ij}}\frac{\partial\Phi_n}{\partial\Sigma_{kl}}]\dot{\Sigma}_{kl} \tag{79}$$

Assuming loading takes place, the inversion of (78) is

$$\begin{aligned}\dot{\Sigma}_{ij} &= [G(\delta_{ik}\delta_{jl}+\delta_{il}\delta_{jk}) + (K-\frac{2}{3}G)\delta_{ij}\delta_{kl} \\ &-(\frac{H\bar{\sigma}^2}{36}+\frac{G}{2\bar{\sigma}^2}\Sigma'_{ij}\Sigma'_{ij}+Ka^2)^{-1}(G\frac{\Sigma'_{ij}}{\bar{\sigma}}+Ka\delta_{ij})(G\frac{\Sigma'_{ij}}{\bar{\sigma}}+Ka\delta_{ij})]\dot{E}_{kl}\end{aligned} \tag{80}$$

where$G = L_P^I/(2+2\upsilon)$ and $K = L_P^I/(3-6\upsilon)$ are shear modulus and bulk modulus, respectively, and

$$a = \frac{1}{2}f\frac{1}{qn+1}\sinh(\frac{3}{2}(\frac{\Sigma_m}{\bar{\sigma}})^{\frac{1}{qn+1}})(\frac{\Sigma_m}{\bar{\sigma}})^{\frac{-qn}{qn+1}} \tag{81}$$

Therefore, this model is fully represented by (61), (65), (67) and (76).

5 Numerical results

The above developed theory will be applied in modeling the constitutive response of porous SMA. One usually studies the porous SMA under the uniaxial compression, because it is hard to analysis the phase distribution under various loadings. Here, we analyzed only under the case of uniaxial compression for simple and the other loading conditions will be discussed in future work. As a simple application of constitutive equations derived, we find the response of porous SMA under uniaxial load with different porosities at isothermal condition. The uniaxial load is

$$\Sigma_{ij} = \begin{bmatrix} 0 & 0 & 0 \\ 0 & 0 & 0 \\ 0 & 0 & \Sigma_{33} \end{bmatrix}$$

To be able to compare the obtained experimental data with modeling predictions, here we use the material parameters of dense Ni-Ti SMA published by Zhao et al (2005) under isothermal temperature. It is well known that porous SMAs have been synthesized using many different methods such as combustion synthesis, hot isostatic processing, and so on. Material constants for porous SMA are unstable and the materials in different experiments are different, and it hard to get the parameter values for porous SMAs with different porosities to theoretical analysis. Hence,

in order to adapt to different porosities, we choose the parameters of dense SMA because it is more stable to get and more applicable than the porous one's. First, it is assumed that the SMA matrix is isotropic with Poisson's ratio $\nu^A = \nu^M = \nu$, the transformation strain hardening constant $\rho b^M = 5.25Mpa$, $\rho b^A = 7Mpa$ by Lagoudas et al. (1996) are adopted. Next, based on the experimental data published by Zhao et al. (2005), the material properties presented in Table 1 have been used during in the numerical calculations. In view of choosing different strain-hardening exponent n in Fig.6, the results demonstrate that $n = 0.4$ is the most close to the experimental data of the porous SMA.

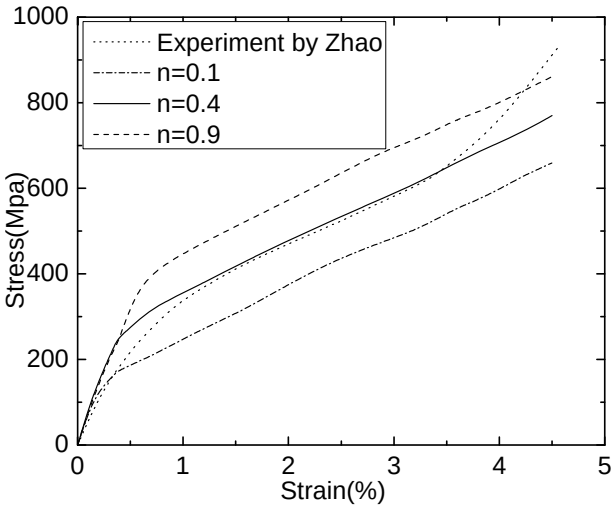

Figure 6: Comparison of model stress-strain curves for strain hardening constants of 0.1, 0.4 and 0.9 for a PVF of 0.13.

Table 1: Parameters used in calculation for porous Ni-Ti SMA by Zhao et al (2005)

ν	L_D^A	L_D^M	$\Sigma_D^{Ms}(\sigma_0 = \sigma_s^M)$	$H_{\max}$	$\Sigma_D^{As}(\sigma_s^A)$	Σ_D^{Af}
0.33	75Gpa	31Gpa	400Mpa	-0.032	600Mpa	300Mpa

Fig.7 shows a comparison between simulation result of the stress-strain response of 13% porosity and experimental data (Zhao et al., 2005) respectively for uniaxial compression. Dot curve represents experimental result published by Zhao et al. (2005). Dash curve is the model result of the literature (Zhao et al., 2005). Solid curve corresponds to the present model. As shown in Fig.7, several observations

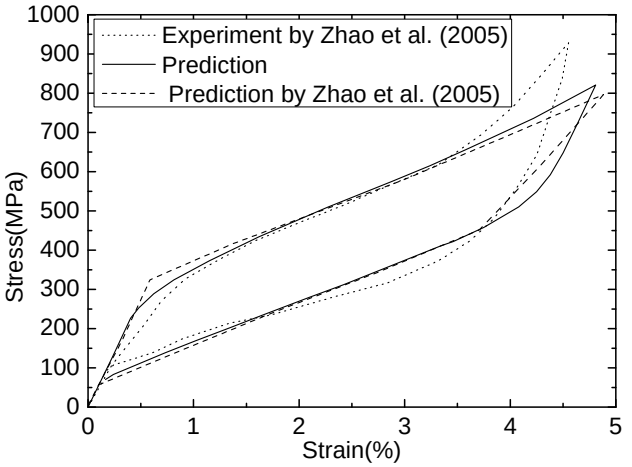

Figure 7: Comparison of model and Zhao's experimental stress-strain curves for strain hardening constant of 0.4 for a PVF of 0.13.

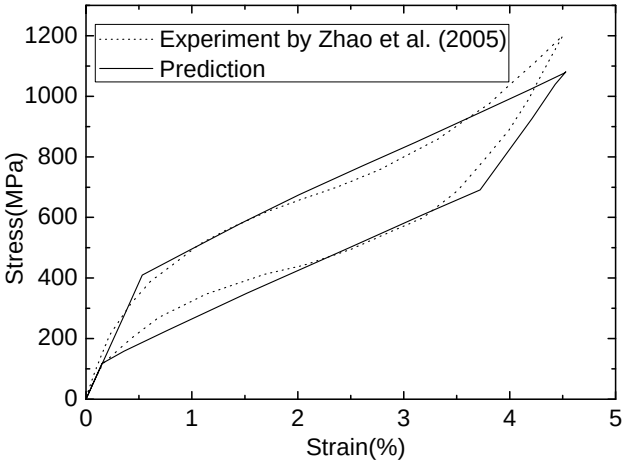

Figure 8: Comparison of model and Zhao's experimental stress-strain curves for a dense SMA specimen.

are made. First, due to the regardless the effect of hydrostatic stress, the point of start transformation in Zhao's model was higher than the experimental value, while the present model is more close to the experiment for considering the counterpart. So the hydrostatic stress plays an important role in the martensitic phase transformation for porous SMA materials. What's more, the behaviors of the mate-

rial during minor loops are also correctly reproduced and verify the validity of the present model. While the nonsymmetry in tension and compression was not considered in this study, because we have a complex derivation and it's hard to derive the complex effective strain for considering it. We will continue to study the model for porous SMA considering the nonsymmetry in tension and compression in the next paper.

When f is zero, the model can be degenerated to model dense SMA. Fig.8 illustrates the measured stress-strain curve and the model prediction of dense Ni-Ti specimen under uniaxial compression. Dot curve represents experimental result published by Zhao et al. (2005), while solid curve corresponds to the present model. From Fig.8 we can obtain that the present research can not only be applied for porous SMA materials, but also be degenerated to dense SMA materials. The present prediction is in good agreement with the experimental data of dense Ni-Ti SMA.

6 Conclusion

Utilizing micromechanics and the upper bound theory, a constitutive model for porous SMA has been developed which can describe the response of both the porous and the dense SMA. The effect of hydrostatic pressure, not accounted for in previous models, has been considered in the present model. The model is then applied to simulate the pseudoelastic behavior of porous SMA with different porosities. Numerical results have been compared with the experimental data (Zhao et al., 2005) has and show good agreement. Importantly, the transformation initiation stress is much closer to the experiment result than simulated by Zhao et al. (2005).

Acknowledgement: The authors acknowledge the financial support of National Natural Science Foundation of China (No. 11172033, 10772021 and 10972027) and National Basic Research Program of China (973 Program) (2010CB7321004). The authors are also very grateful to Dr. D.C. Lagoudas and Dr. Brian Lester, Texas A&M University, USA, for their helpful suggestions.

Appendix A. The solution procedure for macroscopic stresses

In the foregoing analysis we have got the expressions of the macrostresses in (37), (38) and (39). To find the approximate analytic solutions to (37), (38) and (39), we derive the problem in the following part. The volume integral over the sphere is

treated as follows

$$
\begin{aligned}
&dV = r^2 d\Omega dr = r^2 \sin\phi d\phi d\theta dr \quad x = \frac{1}{\lambda} \quad d\lambda = \frac{-1}{x^2} dx \\
&\lambda = (\frac{r}{b})^3, \quad r^2 dr = \frac{b^3}{3} d\lambda \quad \int_\Omega d\Omega = \int_0^{2\pi}\int_0^{\pi} \sin\phi d\phi d\theta \\
&\frac{1}{V}\int_V dV = \frac{3}{4\pi b^3}\int_\Omega \int_a^b r^2 dr d\Omega = \frac{1}{4\pi}\int_\Omega \int_f^1 d\lambda d\Omega \quad \int_f^1 d\lambda = \int_1^{1/f} \frac{1}{x^2} dx
\end{aligned}
\tag{A1}
$$

By using the above, the (37), (38) and (39) now become

$$
\dot{W} = \frac{\sigma_0}{4\pi} \frac{(\dot{E}^{t'}_{mn}\dot{E}^{t'}_{mn})^{(n+1)/2}}{\dot{\varepsilon}_0^n} (\frac{2}{3})^{(n+1)/2} \int_\Omega \int_f^1 Q^{(n+1)/2} d\lambda d\Omega \tag{A2}
$$

$$
\Sigma'_{ij} = \frac{\sigma_0}{6\pi} \frac{(\dot{E}^{t'}_{mn}\dot{E}^{t'}_{mn})^{n/2}}{\dot{\varepsilon}_0^n} (\frac{2}{3})^{n/2} \int_\Omega \int_f^1 Q^{\frac{n-1}{2}} [t_{ij} + D\lambda^{-1}(\delta_{ij} - 3n_i n_j)] d\lambda d\Omega \tag{A3}
$$

$$
\Sigma_{mm} = \frac{\sigma_0}{2\pi} \frac{(\dot{E}^{t'}_{mn}\dot{E}^{t'}_{mn})^{n/2}}{\dot{\varepsilon}_0^n} (\frac{2}{3})^{n/2} \int_\Omega \int_f^1 Q^{\frac{n-1}{2}} (2D\lambda^{-1} - \mu)\lambda^{-1} d\lambda d\Omega \tag{A4}
$$

The volume integral over the matrix is treated as follows

$$
\begin{aligned}
&\lambda = \frac{r^3}{b^3 - a^3}, \quad r^2 dr = \frac{b^3 - a^3}{3} d\lambda, \quad \int_{f/(1-f)}^{1/(1-f)} d\lambda = \int_{1-f}^{(1-f)/f} \frac{1}{x^2} dx \\
&\frac{1}{V_m}\int_{V_m} dV_m = \frac{3}{4\pi(b^3 - a^3)} \int_\Omega \int_a^b r^2 dr d\Omega = \frac{1}{4\pi}\int_\Omega \int_{f/(1-f)}^{1/(1-f)} d\lambda d\Omega
\end{aligned}
\tag{A5}
$$

Then (40) becomes

$$
\bar{\sigma}_e = \frac{\sigma_0}{4\pi} \frac{(\dot{E}^{t'}_{mn}\dot{E}^{t'}_{mn})^{n/2}}{\dot{\varepsilon}_0^n} \int_\Omega \int_{f/(1-f)}^{1/(1-f)} Q^{n/2} d\lambda d\Omega \tag{A6}
$$

where $D = \dot{E}^t_{mm}/3\sqrt{2\dot{E}^{t'}_{kl}\dot{E}^{t'}_{kl}/3}$, $t_{ij} = \dot{E}^{t'}_{ij}/\sqrt{2\dot{E}^{t'}_{kl}\dot{E}^{t'}_{kl}/3} = t_{ij}n_i n_j$, $Q = 1 - 4D\mu/\lambda + 4D^2/\lambda^2$.

The integrals over x can be put in terms of the following functions

$$\int_1^{1/f} \frac{Q^{(n-1)/2}}{x^2} dx = F(x,\mu), \quad \int_1^{1/f} \frac{Q^{(n-1)/2}}{x} dx = G(x,\mu), \quad \int_1^{1/f} Q^{(n-1)/2} dx = H(x,\mu) \tag{A7}$$

$$\frac{x}{2} Q^{(n+1)/2} \,|_1^{1/f} = I(x,\mu), \quad Q^{(n+1)/2} \,|_1^{1/f} = J(x,\mu), \tag{A8}$$

Then (A2), (A3), (A4) and (A6) become

$$\dot{W} = \frac{\sigma_0}{4\pi} \frac{(\dot{E}^{t'}_{mn}\dot{E}^{t'}_{mn})^{(n+1)/2}}{\dot{\varepsilon}_0^n} (\frac{2}{3})^{(n+1)/2} \int_\Omega \int_f^1 [(\frac{x}{2} - \frac{\mu}{4D}) Q^{(n+1)/2} + \frac{1-\mu^2}{2} H(x,\mu)\,]|_1^{1/f} d\Omega \tag{A9}$$

$$\Sigma'_{ij} = \frac{\sigma_0}{6\pi} \frac{(\dot{E}^{t'}_{mn}\dot{E}^{t'}_{mn})^{n/2}}{\dot{\varepsilon}_0^n} (\frac{2}{3})^{n/2} \int_\Omega [t_{ij} F(x,\mu) + D(\delta_{ij} - 3n_i n_j) G(x,\mu)]\big|_1^{1/f} d\Omega \tag{A10}$$

$$\Sigma_{mm} = \frac{\sigma_0}{2\pi} \frac{(\dot{E}^{t'}_{mn}\dot{E}^{t'}_{mn})^{n/2}}{\dot{\varepsilon}_0^n} (\frac{2}{3})^{n/2} \int_\Omega [2DH(x,\mu) - \mu G(x,\mu)]|_1^{1/f} d\Omega \tag{A11}$$

$$\bar{\sigma}_e = \frac{\sigma_0}{4\pi} \frac{(\dot{E}^{t'}_{mn}\dot{E}^{t'}_{mn})^{n/2}}{\dot{\varepsilon}_0^n} \int_\Omega K(x,\mu)|_{1-f}^{(1-f)/f} d\Omega \tag{A12}$$

For the sake of finding the approximate analytic solutions to (A9), (A10), (A11) and (A12), we define

$$\bar{F}^{(i)} = \Big(F^{(i)}(x,\mu)\Big)_{\mu=0} \Big|_{x=1}^{x=\frac{1}{f}}, \quad \bar{K}^{(i)} = \Big(K^{(i)}(x,\mu)\Big)_{\mu=0} \Big|_{x=1-f}^{x=\frac{1-f}{f}} \tag{A13}$$

There are the same format for $\bar{G}^{(i)}\bar{H}^{(i)}\bar{I}^{(i)}\bar{J}^{(i)}$. Moreover, we expand the functions F, G, H, I, J, and K in μ around $\mu = 0$, and afterwards integrate over Ω.

Thus the expansions are of the form

$$F(x,\mu)|_1^{1/f} = \bar{F}^{(0)} + \mu\bar{F}^{(1)} + \frac{1}{2}\mu^2\bar{F}^{(2)} + \cdots \tag{A14}$$

$$K(x,\mu)|_{1-f}^{(1-f)/f} = \bar{K}^{(0)} + \mu\bar{K}^{(1)} + \frac{1}{2}\mu^2\bar{K}^{(2)} + \cdots \tag{A15}$$

As a result, the approximate stress integrals become to the second order in μ

$$\dot{W} = \frac{\sigma_0}{4\pi}\frac{(\dot{E}^{t'}_{mn}\dot{E}^{t'}_{mn})^{(n+1)/2}}{\dot{\varepsilon}_0^n}(\frac{2}{3})^{(n+1)/2}\int_\Omega [-\frac{\mu}{4D}(\bar{J}^{(0)}+\mu\bar{J}^{(1)}+\frac{1}{2}\mu^2\bar{J}^{(2)}) + \frac{1-\mu^2}{2}(\bar{H}^{(0)}+\mu\bar{H}^{(1)}+\frac{1}{2}\mu^2\bar{H}^{(2)})+\bar{I}^{(0)}+\mu\bar{I}^{(1)}+\frac{1}{2}\mu^2\bar{I}^{(2)}]d\Omega \tag{A16}$$

$$\Sigma'_{ij} = \frac{\sigma_0}{6\pi}\frac{(\dot{E}^{t'}_{mn}\dot{E}^{t'}_{mn})^{n/2}}{\dot{\varepsilon}_0^n}(\frac{2}{3})^{n/2}\times \int_\Omega [t_{ij}(\bar{F}^{(0)}+\mu\bar{F}^{(1)}+\frac{1}{2}\mu^2\bar{F}^{(2)})+D(\delta_{ij}-3n_in_j)(\bar{G}^{(0)}+\mu\bar{G}^{(1)}+\frac{1}{2}\mu^2\bar{G}^{(2)})]d\Omega \tag{A17}$$

$$\Sigma_{mm} = \frac{\sigma_0}{2\pi}\frac{(\dot{E}^{t'}_{mn}\dot{E}^{t'}_{mn})^{n/2}}{\dot{\varepsilon}_0^n}(\frac{2}{3})^{n/2}\int_\Omega (2D(\bar{H}^{(0)}+\mu\bar{H}^{(1)}+\frac{1}{2}\mu^2\bar{H}^{(2)})-\mu(\bar{G}^{(0)}+\mu\bar{G}^{(1)}))d\Omega \tag{A18}$$

$$\bar{\sigma}_e = \frac{\sigma_0}{4\pi}\frac{(\dot{E}^{t'}_{mn}\dot{E}^{t'}_{mn})^{n/2}}{\dot{\varepsilon}_0^n}\int_\Omega \bar{K}^{(0)}+\mu\bar{K}^{(1)}+\frac{1}{2}\mu^2\bar{K}^{(2)}d\Omega \tag{A19}$$

Neglecting the smaller terms and carrying out the integral over Ω give

$$\dot{W} = \frac{\sigma_0(\dot{E}^{t'}_{mn}\dot{E}^{t'}_{mn})^{(n+1)/2}}{\dot{\varepsilon}_0^n}(\frac{2}{3})^{(n+1)/2}(\bar{I}^{(0)}+\frac{1}{10}\bar{I}^{(2)}-\frac{1}{20D}\bar{J}^{(1)}+\frac{2}{5}\bar{H}^{(0)}+\frac{1}{20}\bar{H}^{(2)}) \tag{A20}$$

$$\frac{\Sigma'_{ij}}{\sigma_0} = \frac{(\dot{E}^{t'}_{mn}\dot{E}^{t'}_{mn})^{n/2}}{\dot{\varepsilon}_0^n}(\frac{2}{3})^{n/2}t_{ij}(\frac{2}{3}\bar{F}^{(0)}+\frac{1}{15}\bar{F}^{(2)}) \tag{A21}$$

$$\frac{\Sigma_{mm}}{\sigma_0} = \frac{(\dot{E}^{t'}_{mn}\dot{E}^{t'}_{mn})^{n/2}}{\dot{\varepsilon}_0^n}(\frac{2}{3})^{n/2}(4D\bar{H}^{(0)}+\frac{2D}{5}\bar{H}^{(2)}-\frac{2}{5}\bar{G}^{(1)}) \tag{A22}$$

$$\bar{\sigma}_e = \sigma_0\frac{(\dot{E}^{t'}_{mn}\dot{E}^{t'}_{mn})^{n/2}}{\dot{\varepsilon}_0^n}(\bar{K}^{(0)}+\frac{2}{5}\bar{K}^{(2)}) \tag{A23}$$

References

Auricchio. F., Conti. M., Morganti. S., Reali. A. (2010): Shape Memory Alloy: from Constitutive Modeling to Finite Element Analysis of Stent Deployment. *CMES: Computer Modeling in Engineering & Sciences* 57(3), 225-244.

Arghavani. J., Auricchio. F., Naghdabadi. R. (2011): A finite strain kinematic hardening constitutive model based on Hencky strain: General framework, solution algorithm and application to shape memory alloys. *Int. J. Plast.* 27,940-961.

Birman, V., (1997): Review of mechanics of shape memory alloy structures. *Appl. Mech. Rev.* 50, 629-645.

Boyd, J.G., Lagoudas, D.C., (1994): Thermomechanical response of shape memory composites. *J. Intell. Mater. Syst. Struct.* 5, 333-346.

Entchev, P.B., Lagoudas, D.C., (2002): Modeling porous shape memory alloys using micromechanical averaging techniques. *Mech. Mater.* 34, 1-24.

Entchev, P.B., Lagoudas, D.C., (2004): Modeling of transformation induced plasticity and its effect on the behavior of porous shape memory alloys. Part II: porous SMA response. *Mech. Mater.* 36, 893-913.

Garner, L.J., Wilson, L.N., Lagoudas, D.C., Rediniotis, O.K., (2000): Development of a shape memory alloy actuated biomimetic vehicle. *Smart Mater. Struct.* 9 , 673–683.

Greiner, C., Oppenheimer, S.M., Dunand, D.C., (2005): High strength, low stiffness, porous Ni-Ti with superelastic properties. *Acta Biomater.* 1, 705-716.

Gurson, A.L. (1977): Continuum theory of ductile rupture by void nucleation and growth Part I. Yield cirteria and flow rules for porous media. *J. Eng. Mater. Technol.* 99, 2-15.

Gyunter, V.E., Sysoliatin, P., Temerkahamor, T., (1995): Superelastic shape memory implants in maxillofacial surgery, traumatology, orthopedics, and neurosurgery. Tomsk university publishing house, Tomsk.

Huang, Y., (1991): Accurate dilatation rate for spherical voids in triaxial stress fields. *J. Appl. Mech.* 58, 1084-1086.

Ilyin, A., Dudin, M., Makarova, I., (1995): NiTi instruments for TMJ surgeries. In: Conf. Proc. Superelastic shape memory Implants in Medicine. Tomsk, pp. 61-62.

Jardine, A.P., Kudva, J.M., Martin, C., Appa, K., (1996): Shape memory alloy Ti-Ni actuators for twist control of smart wing designs. In: SPIE Proc. Mathematics and control in smart structures, 2717, 160-165.

Jeong, H.Y., Pan, J., (1995): A macroscopic constitutive law for porous solids

with pressure-sensitive matrices and its implications to plastic flow localization. *Int. J. Solids. Struct.* 32, 3669-3691.

Kim, J.H., Kang, T. J., Yu, W. R., (2010): Thermo-mechanical constitutive modeling of shape memory polyurethanes using a phenomenological approach. *Int. J. Plast.* 26, 204-218.

Lagoudas, D.C., Bo, Z., Qidwai, M.A., (1996): A unified thermodynamic constitutive model for SMA and finite element analysis of active metal matrix composites. *Mech. Compos. Mater. Struct.* 3, 153-179.

Levitas, V. I., Ozsoy, I. B., (2009): Micromechanical modeling of stress-induced phase transformations. Part 2. Computational algorithms and examples. *Int. J. Plast.* 25, 546-583.

Levitas, V. I., Levin, V. A., Zingerman, K. M., Freiman, E. I., (2009): Displacive phase transitions at large strains: Phase-field theory and simulations. PRL 103, 025702.

Li, B.Y., Rong, L.J., Li, Y.Y., Gjunter, V.E., (2000): Synthesis of porous Ni-Ti shape memory alloys by SHS: Reaction mechanism and anisotropy in pore structure. *Acta. mater.* 48, 3895-3904.

Li, Y.H., Rong, L.J., Li, Y.Y., (2001): Pore characteristics of porous NiTi alloy fabricated by combustion synthesis. *J. Alloys Compd.* 325, 259-262.

Liang, C., Davidson, F., Scjetky, L.M., Straub, F.K., (1996): Applications of torsional shape memory alloy actuators for active rotor blade control: opportunities and limitations. In: SPIE Proc. Mathematics and Controls in Smart Structures, 2717, 91-100.

Lipscomb, I.P., Nokes, L.D.M., (1996): The application of shape memory alloys in medicine. Mechanical Engineering Publications, suffold.

Liu, B.F., Dui, G.S., Zhu, Y.P., (2011): Effects of hydrostatic stress on porous shape memory alloy transformation. *Journal of Beijing Jiaotong University*. 35(4):120-124. (In Chinese)

Liu, Y., Humbeeck, J.V., Stalmans, R., Delaey, L., (1997): Some aspects of the properties of NiTi shape memory alloy. *J. Alloys Compd.* 247, 115-121.

Martynova, I., Skorohod, V., Solonin, S., Goncharuk, S., (1991): Shape memory and superelasticity behaviour of porous Ti-Ni material. *J. Phys. IV.* 01, 421-426.

Mochida, T., Taya, M., Lloyd, D.J., (1991): Fracture of particles in a particle/metal matrix composite under plastic straining and its effects on the young's modulus of the composite. *Mater. Trans. JIM*. 32, 931-942.

Nemat-Nasser, S., Su, Y., Guo, W.G.., Isaacs, J., (2005): Experimental characterization and micromechanical modeling of superelastic response of a porous Ni-Ti

shape memory alloy. *J. Mech. Phys. Solids.* 53, 2320-2346.

Pan, H., Thamburaja, P., Chau, F. S., (2007): Multi-axial behavior of shape-memory alloys undergoing martensitic reorientation and detwinning. *Int. J. Plast.* 23, 711-732.

Panico. M., Brinson, L.C., (2008): Computational modeling of porous shape memory alloys. *Int. J. Solids. Struct.* 45, 5613-5626.

Peng, X., Pi, W., Fan, J., (2008): A micro structure-based constitutive model for the pseudoelastic behavior of NiTiSMAs. *Int. J. Plast.* 24, 966-990.

Phillips. F.R., Dong. F., Zheng. H.X., Lagoudas. D.C. (2011): Phase transformation in free-standing SMA nanowires. *Acta. Mater.* 59(5), 1871-1880.

Qidwai, M.A., Entchrv, P.B., Lagoudas, D.C., DeGiorgi, V.G., (2001): Modeling of the themomechanical behavior of porous shape memory alloys. *Int. J. Solids. Struct.* 38, 8653-8671.

Qidwai, M.A., Lagoudas, D.C., (2000): On thermomechanics and transformation surfaces of polycrystalline NiTi shape memory alloy material. *Int. J. Plast.* 16, 1309-1343.

Otsuka, K., Ren, X.B., (1999): Recent developments in the research of shape memory alloys. *Intermetallics.* 7, 511-528.

Qu, J.M., Cherkaoui, M., (2006): Fundamentals of micromechanics of solids. John Wiley & Sons, Inc. New Jersey.

Shen, H., Brinson, L.C., (2007): Finite element modeling of porous titanium. *Int. J. Solids Struct.* 44, 320-335.

Starosvetsky, D., Gotman, I., (2001): Corrosion behavior of titanium nitride coated Ni-Ti shape memory surgical alloy. *Biomaterials.* 22, 1853-1859.

Tanaka, K. (1986): A thermomechanical sketch of shape memory effect: one dimensional tensile behavior. *Res Mech.* 18, 251-263.

Taya, M., Furuya, Y., Yamada, Y., Watanabe, R., Shibata, S., Mori, T., (1993): Strengthening mechanisms of NiTi shape memory fiber/Al matrix composite. In: Varadan, V. (Ed), *Proc. Smart Marterials*, vol. 1916, 373-383.

Teppei, W., Yoshimi, W., Hiroshi, O., (2005): Development of Fe-Mn-Si-Cr shape memory alloy fiber reinforced plaster-based smart composites. *Mater. Sci. Forum.* 475, 2063-2066.

Tvergaard, V., (1981): Influence of voids on shear band instabilities under plane strain conditions. *Int. J. Fract.* 17, 389–407.

Wang. X.M., Xu. B.X., Yue. Z.F. (2008): Micromechanical modelling of the effect of plastic deformation on the mechanical behaviour in pseudoelastic shape

memory alloys. *Int. J. Plast.* 24,1307-1332.

Wang, Z.P., Lam, K.Y., Cotterell, B., (1995): An approximate yield criterion for voided nonlinear materials. *Mech. Mater.* 22, 291-300.

Zhao, Y., Taya, M., Kang, Y.S., Kawasaki, A., (2005): Compression behavior of porous Ni-Ti shape memory alloy. *Acta. Mater.* 53, 337-343.